Jurnal Kejuruteraan 35(2) 2023: 361-374
https://doi.org/10.17576/jkukm-2023-35(2)-07

Structure-preserving Contrast Enhancement of Fundus Images using Dualistic Sub-Image Bi-histogram Bezier Curve

Kelvin Chia Hiik Ling[a], Tan Tian Swee[a]*, Yan Chai Hum[b], Wan Hazabbah Wan Hitam[c], Muhammad Amir As'ari[a], Abdul Asnida Wahab[a], Jia Hou Tan[d], Kah Meng Leong[e], Joyce Sin Yin Sia[a], Matthias Foh Thye Tiong[a], Sameen Ahmed Malik[a], Sinan S. Mohammed Sheet[a] & Roy Eduardo Aquilar Leon[f]

[a]*School of Biomedical Engineering and Health Science, Universiti Teknologi Malaysia, Johor Bahru, Malaysia*
[b] *Department of Mechatronics and Biomedical Engineering, Universiti Tunku Abdul Rahman, Kajang, Malaysia*
[c] *Department of Ophthalmology, Universiti Sains Malaysia, Kubang Kerian, Malaysia*
[d] *The Institution of Engineering and Technology, United Kingdom*
[e] *Department of Electrical & Electronic Engineering, Southern University College, Johor Bahru, Malaysia*
[f] *Faculty of Electrical and Computer Engineering, Escuela Superior Politecnica del Litoral, Guayaquil, Ecuador*

**Corresponding author: tantswee@biomedical.utm.my*

Received 22 March 2022, Received in revised form 18 August 2022
Accepted 18 September 2022, Available online 30 March 2023

ABSTRACT

Diabetic retinopathy is a common eye disease among diabetic patients which is caused by excessive sugar in the blood vessels that damage the retina. Fundus images are retina images that are captured and diagnosed by ophthalmologists. Ophthalmologists diagnose the progressive stages of diabetic retinopathy so that early detection of pre-diabetic retinopathy can be carried out. However, the quality of the fundus image can be associated with the brightness of the background and the indistinctive vessel contrast. This paper presents a novel extension of Bi-histogram Bezier curve contrast enhancement (BBCCE) based on the mean partition of its histogram. The disadvantage of having mean as the threshold partition is that the histogram distribution can be skewed due to an outlier The proposed Dualistic Sub-Image Bi-histogram Bezier Curve Contrast Enhancement (DSI-BBCCE) method partitions the original histogram into two, using the median of the active dynamic intensity range of the input image and process two Bezier transform curves separately to replace the original cumulative density function curve as the median is not affected by the outlier This DSI-BBCCE has the advantage of preserving the structure, median brightness and preventing over enhancement. The result shows that DSI-BBCCE has achieved a power signal to noise ratio (PSNR) of 20.08±0.94 dB, absolute mean brightness error (AMBE) of 20.15±1.89, structural similarity index model (SSIM) of 0.8096±0.0185, structure measure operator (SMO) of 3.2±1.10 and lightness measure order (LMO) of 200.90±44.19.

Keywords: Diabetic retinopathy; Fundus; Median Brightness; Bi-histogram; DSI-BBCCE; Bezier

INTRODUCTION

Diabetes mellitus is a common metabolic disorder faced by many, which is caused by the presence of high blood glucose in the blood (Ogurtsova et al. 2017). From the World Health Organization (WHO) global report, the number of adults with diabetes has increased significantly since 1980 to 2014 (Lovic et al. 2020). According to the National Health and Morbidity Survey (NHMS) in 2019, there are about 49% of Malaysians had diabetes but they had never gone through examination and diagnosis with the chronic disease (WHO 2021). Diabetes can lead to complications in many parts of the body and increase the risk of dying prematurely such as stroke, blindness, heart attack, kidney failure (Teh, Lim, Jusoh, Osman, & Mualif 2021) and amputation (WHO 2021). Diabetic retinopathy is a complication of diabetes mellitus in a long run in which the retinal vessel level is damaged (Bowling 2015). The damaged retinal vessel can cause blurriness vision and near blindness if left undiagnosed and untreated (Wykoff et al. 2021). The diabetic retinopathy is caused by high concentration of glucose that is present in the blood vessels and at the same time block the tiny blood vessels that nourish the retina. As a result, its blood supply is cut. Contrary to age-related macular degeneration (AMD), it is caused by aging process and is one of the multiple current daunting aging diseases (Teh, Mualif, & Lim 2021).

Diabetic retinopathy is diagnosed through the fundus images captured during funduscopy examinations. The quality of the fundus image will consequently affect the diagnosis of early detection of diabetic retinopathy from the thickness of the retinal blood vessel near the optic disc (Knudtson et al. 2003). Diabetic retinopathy can be classified into non-proliferative diabetic retinopathy (NPDR) and proliferative diabetic retinopathy (PDR). NPDR has the visible features such as one or more microaneurysms, haemorrhages or exudates (Lai, Wong, & Liew, 2019). PDR

is the more advanced form of the disease and has the feature of neovascularization which is new abnormal formation of blood vessel growth. The dilation of the venules and the generalized arteriolar narrowing which are parameters of ischemic stroke are associated with diabetic retinopathy (N. Cheung et al. 2007). After that, researches are conducted to study the relationship between retinal vascular geometry with diabetes and diabetic retinopathy (C. Y.-l. Cheung et al. 2012).

Diagnosis of retinal diseases based on digital fundus images are not only based on the ability of the observers or ophthalmologists to differentiate between the vein and the artery from the background. Other abnormalities are present in the fundus images such as cotton wool, microaneurysms, exudates, haemmorhages, drusen as well as the brightness of the vessel reflects. Thus, the quality of the images is crucial to show the visible features and vessel thickness as it may abolish the appearance of these abnormalities. Nevertheless, fundus image enhancement is an essential and challenging pre-processing step for automated diagnosis of ocular disorders.

LITERATURE REVIEW

CONTRAST ENHANCEMENT

Contrast enhancement is one of the most important steps in processing the fundus image for vessel segmentation (Tian-Swee, Ameen, Hitam, Hum, & Teoh, 2017). Although the simplest contrast enhancement is the histogram equalization (HE), it causes amplification of noise and thus over-enhance the image in two distinct regions (Chai, Swee, Seng, & Wee, 2013). To overcome this, adaptive histogram equalization (AHE) is introduced so that the image 's brightness is redistributed equally, by using spatial filtering desplte in two distinctive regions. A new improved version of AHE which is contrast limited adaptive histogram equalization (CLAHE) introduced an interactive intensity windowing that allows the detection of small intensity changes and thus reduces the noise (Yin et al. 2020). In the year 1997, mean brightness preservation is introduced by dividing input histogram images into two sub histograms images with mean as the threshold level by Kim so as to give a more natural enhancement (Kim, 1997). This technique is called Bi-histogram equalization (BBHE). From there, different techniques are implemented and improvised in the bi-histogram equalization. In 1999, equal area dualistic sub image histogram equalization (DSIHE) is introduced by Wang et al in which input image is divided by two equal-size histograms based on the median threshold (Wang, Chen, & Zhang, 1999). In 2014, Gan proposed the utilization of Bezier curve in the cumulative density function (CDF) curve on BBHE method in medical images such as MRI knee images which have indistinctive tissue contrast and poor background luminance (Gan et al. 2014). This method is called Bi-histogram Bezier curve contrast enhancement (BBCCE). After that, in 2020, Joyce proposed prominent region of interest contrast enhancement (PROICE) to separate the input image into two Gaussians that cover the dark region pixels and bright region pixels respectively (Yin et al. 2020). The threshold level is based on the mean of the brighter Gaussian region which is the second Gaussian and where the region of interest is situated. Since BBCCE divides the input image histograms based on the mean threshold, as an extension of BBCCE, DSI-BBCCE is proposed based on the median threshold which is not affected by a few large values that drive the mean upward and a few small values that drive the mean downward.

METHODOLOGY

FUNDUS IMAGE ACQUISITION

The fundus images are acquired from Digital Retinal Images for Vessel Extraction (DRIVE) database. A Canon CR5 non-mydriatic 3CCD camera with a 45-degree field of view (FOV) is used to acquire the images. The images are captured using 8-bits per color plane at 768 by 584 pixels. The set of 40 images, which are 20 test and 20 training images of fundus, will be the input images. The details of the DRIVE database can be acquired from this website: https://drive.grand-challenge.org/

DUALISTIC SUB-IMAGE BI-HISTOGRAM BEZIER CURVE

The cumulative density function (CDF) derives the traditional transform curve. Bezier functions to stretch the original intensity distribution in the transform curve. This is to endure the full dynamic range of the image is covered.

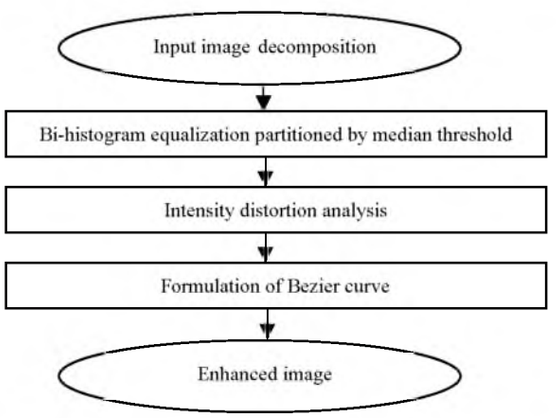

FIGURE 1. Flowchart of DSI-BBCCE

Firstly, the input image is decomposed into bins of histogram which consists of L discrete gray levels labelled as $X = \{X(i,j)\}$, where $X_k(i,j) \in \{X_0, X_1, ..., X_{L-1}$ Histogram of n_k against X_k is plotted. The pixel intensities are assumed as random variables in which each level is measured in the form of a probability density function. The probability density function is denoted as the pixel occurrence of certain gray level, n_k divided by total number of pixels in the image, n in Equation 1. A histogram graph of n^k agalnst X_k is plotted.

$$p(X_k) = \frac{n^k}{n} \quad (1)$$

where:
$k = 0,1, \ldots, L\text{-}1$,
n^k represents the number of times that the level X_k appears in the input image X,
n is the total number of samples in the input image.

Secondly, the histogram image distribution is partitioned into two sub-images which are also two sub-histograms based on the threshold median value. This method is known as bi-histogram equalization. The median threshold is denoted as CDF equal to 0.5 and is chosen so that any sudden distribution skew due to larger amounts of background pixels to lower histogram can be confined. The equation for the median is as follows:

$$I_{med} = round\left(\frac{I_{max} - I_{min}}{2}\right) \quad (2)$$

Equation 3 shows the cumulative density function (CDF).

$$c(x) = \sum_{j=0}^{k} p(X_k) \quad (3)$$

A transform function can be formed based on the CDF and is shown in Equation 4.

$$f(x) = X_0 + (X_{L-1} - X_0)c(x) \quad (4)$$

Severe intensity distortion can happen if there is an abrupt increase in the CDF curve. With that, the solution is to smoothen the CDF curve. Absolute intensity difference (AID) is an indicator of the degree of contrast enhancement which can be shown in Equation 5. The lower the AID, the lower the degree of contrast enhancement and vice versa.

$$AID = x' - x \quad (5)$$

where:
x' is transformed intensity distribution and is the original intensity distribution

Computing discrete AIDs can deduce the intensity difference curves so that the critical points are obtained to form the Bezier transform curve. Intensity distribution and the intensity fluctuation resultant can affect the formulation of the transform curve. The intensity difference curve is denoted in Equation 6.

$$y = I(x) \quad (6)$$

Intensity discrepancy value (IDV) is a group of real numbers which corresponds with the critical points in which the gradient, $\frac{dy}{dx}$ is equal to zero. The critical points, P(x) can be either minimum local points when $\frac{d^2y}{dx^2} > 0$ and or maximum local points when $\frac{d^2y}{dx^2} < 0$. By locating the largest IDV, the global maximum and minimum can be determined within the respective denoted constraints:

$$P_{Global\ maximum} = \begin{cases} Argmax(IDV); y > 0 \\ 0 \quad ; otherwise \end{cases} \quad (7)$$

$$P_{Global\ minimum} = \begin{cases} Argmin(IDV); y < 0 \\ 0 \quad ; otherwise \end{cases} \quad (8)$$

where:
Argmax (IDV) is $P_{Global\ maximum}$ when $y > 0$ while
Argmin (IDV) is $P_{Global\ minimum}$ when $y < 0$

IDVs are calculated from the two sub-histogram images and thus two pair of critical points are obtained.

Bezier curve is similar to the convex hull in exception the curve is contained internally in the polygon, at the same time, in its control polygon, the generated curve does not derail off. The characteristic of a Bezier curve is that it is smoother than the traditional CDF curve. This smoothness characteristic generates smaller AID. Bezier curve equation is denoted in Equation 9.

$$Q(t) = \sum_{i=0}^{n} B_{n,i}(t)P_i \quad (9)$$

where:
P_i are control points which are within the domain $t \in$ boundary [0,1] boundary and $B_{n,i}(t)$ is the Bernstein Polynomial that can be shown in Equation 10.

$$B_{n,i}(t) = \binom{n}{i} t^i (1-t)^{n-i} \quad (10)$$

in which the Binomial coefficient $\binom{n}{i}$ is as denoted:

The number of global extrema detected indirectly determine the degree of Bezier curve and number of control points. For example, a third-degree Bezier curve, which has 4 control points $P_i \in \{P_1, P_2, P_3, P_4\}$, has a pair of global extrema. Another example, is that if a Bezier curve is a second degree, it will have 3 control points $P_i \in \{P_1, P_2, P_3\}$.

The proposed DSI-BBCCE framework, which is a novel extension of BBCCE, is as shown below.

(a)

(b)

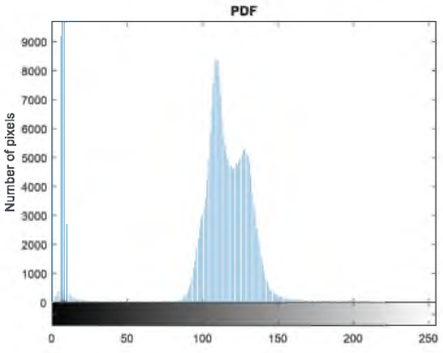
PDF
Number of pixels
Intensity

(c)

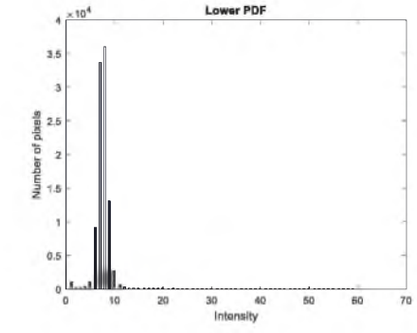
Lower PDF
Number of pixels
Intensity

(d)

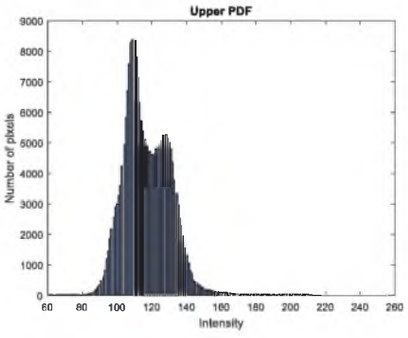
Upper PDF
Number of pixels
Intensity

(e)

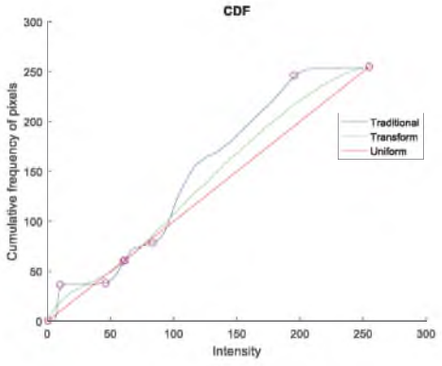
CDF
Cumulative frequency of pixels
Intensity
Traditional
Transform
Uniform

(f)

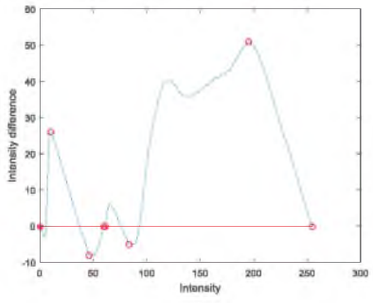
Intensity difference
Intensity

(g)

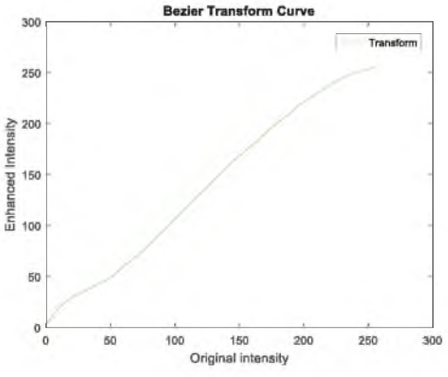
Bezier Transform Curve
Transform
Enhanced Intensity
Original intensity

(h)

(i)

FIGURE 2. DSI-BBCCE framework: (a) Original image, (b) Grayscale image, (c) Histogram image (d) Lower sub histogram, (e) Upper sub histogram, (f) CDF graph, (g) Intensity discrepancy curve, (h) Bezier transform curve, (i) Enhanced image.

IMAGE QUALITY ASSESSMENT METHODOLOGY

The images are tested using the following methods such as HE, AHE, CLAHE, BBCCE and DSI-BBCCE. The performance of preservation and contrast enhancement of each resultant images is evaluated. Statistical analysis in terms of peak signal-to-noise ratio (PSNR), absolute mean brightness error (AMBE), structural similarity index model (SSIM), structure measure operator (SMO) and lightness measure order (LMO).

Firstly, PSNR defines the ratio of maximum possible intensity value of input image to mean squared error (MSE). Mean squared error (MSE) is also defined as the average squares of the errors between the input and output images. The equation of PSNR is as shown below:

$$PSNR = 10\log_{10}\left(\frac{{l_{in}}^{max^2}}{MSE}\right) \tag{12}$$

$$= 20\log_{10}\left(\frac{{l_{in}}^{max}}{MSE}\right) \tag{13}$$

The equation of MSE is as follows:

$$\text{MSE} = \frac{1}{M \times N}\sum_{a=1}^{M}\sum_{b=1}^{N}[I_{ori}(a,b) - I_{en}(a,b)]^2 \tag{14}$$

MSE is always positive due to its squared characteristic. The smaller the MSE, the better the result. It is because the error is at its minimum. The higher the PSNR, the better the quality of the enhanced image.

Secondly, Absolute mean brightness error (AMBE) measures the brightness preservation of the output image.

$$AMBE = \frac{\left|Mean_{I_{ori}} - Mean_{I_{en}}\right|}{L} \tag{15}$$

where:
L is the dynamic range of the input image

$$L = {I_{in}}^{max} - {I_{in}}^{min} \tag{16}$$

The smaller the AMBE, the better the preservation of the image.

Thirdly, Structural similarity index model (SSIM) measures the similarity between original image and enhanced image. SSIM consists of three comparison measurements which are luminance (L), contrast (C) and structure (S). Original image is denoted as a 'x' subscript while enhanced image as 'y' subscript.

$$Luminance\ comparison, L(x,y) = \frac{2\mu_x\mu_y + c_1}{{\mu_x}^2 + {\mu_y}^2 + c_1} \tag{17}$$

$$Contrast\ comparison, C(x,y) = \frac{2\sigma_x\sigma_y + c_2}{{\sigma_x}^2 + {\sigma_y}^2 + c_2} \tag{18}$$

$$Structure\ comparison, S(x,y) = \frac{\sigma_{xy} + c_3}{\sigma_x\sigma_y + c_3} \tag{19}$$

where:

μ_x = average of original image,

μ_y = average of enhanced image,

${\sigma_x}^2$ = variance of original image,

${\sigma_y}^2$ = variance of enhanced image

$\sigma_x\sigma_y$ = covariance of original and enhanced image

$c_1 = (k_1L)^2$, $c_2 = (k_2L)^2$, $c_3 = c_2/2$ are variables that stabilize the division with weak denominator,

where:

$k_1 = 0.01$ and $k_2 = 0.03$ by default,

L is the dynamic range of the pixel values

The combined weighed comparative measure is as shown below:

$$SSIM(x,y) = [L(x,y)^{\alpha} \cdot C(x,y)^{\beta} \cdot S(x,y)^{\gamma}] \tag{20}$$

Setting the weights α, β and γ equal to 1, the formula can be reduced to the equation shown below:

$$SSIM(x,y) = \frac{(2\mu_x\mu_y + c_1)(2\sigma_{xy} + c_2)}{(\mu_x^2 + \mu_y^2 + c_1)(\sigma_x^2 + \sigma_y^2 + c_2)} \tag{21}$$

The higher the value of SSIM, the more the similarity between original image and enhanced image.

There are two method assessments which measure the performance of natural preservation which are Structure Measure Operator (SMO) and Lightness Measure Order (LMO). SMO is an over-enhancement metric which tries to capture the structural change while LMO is an over-

enhancement measure that is based on local inversion (Khan, Beghdadi, Cheikh, Kaaniche, & Qureshi 2020).

SMO computes the structural difference in terms of homogeneity value of original image, HO_{ij}^{o}, and enhanced image, HO_{ij}^{e} in relative to the original image, HO_{ij}^{o}.

$$SMO\ (x,y) = \frac{1}{M \times N} \sum_{i=1}^{M} \sum_{j=1}^{N} \frac{|HO_{ij}^{o} - HO_{ij}^{e}|}{HO_{ij}^{o}} \tag{22}$$

where HO_{ij} is defined as the product of three quantities of edge value, E_{ij}, entropy, H_{ij} and standard deviation, V_{ij} in a $d \times d$ window around a pixel (Ismail, Chen, Ng, & Ramli, 2016).

$$HO_{ij} = E_{ij} \times V_{ij} \times H_{ij} \tag{23}$$

where entropy is as follows;

$$E_{ij} = \sqrt{S_{1ij}^{2} + S_{2ij}^{2}} \tag{24}$$

where S_1 and S_2 is the row and column mask based on the Sobel operator.

Standard deviation of image

$$V_{ij} = \sqrt{\frac{1}{d^2} \sum_{p=i-\frac{d-1}{2}}^{i+\frac{d-1}{2}} \sum_{q=j-\frac{d-1}{2}}^{j+\frac{d-1}{2}} (g_{pq} - m_{ij})^2} \tag{25}$$

where the value of mean intensity, m_{ij}

$$m_{ij} = \frac{1}{d^2} \sum_{p=i-\frac{d-1}{2}}^{i+\frac{d-1}{2}} \sum_{q=j-\frac{d-1}{2}}^{j+\frac{d-1}{2}} g_{pq} \tag{26}$$

The smaller the SMO, the better the preservation of the image.

LMO equation is as shown below:

$$LMO = \frac{1}{M \times N} \sum_{i=1}^{M} \sum_{j=1}^{N} \left| [d_e(i,j) - d_o(i,j)] \cdot \left[\frac{sign(d_e(i,j)) - sign(d_o(i,j))}{2} \right] \right| \tag{27}$$

where;

$d_o(i,j)$ is the difference between pixel values (i,j) of the original image and its local mean filter of window size of 31×31,

$d_e(i,j)$ is the difference between pixel values (i,j) of the enhanced image and its local mean filter of window size of 31×31,

$sign(.)$ is the signum function. Signum function is as follows:

$$f(x) = \begin{cases} 1, & x > 0 \\ 0, & x = 0 \\ -1, & x < 0 \end{cases} \tag{28}$$

The smaller the LMO, the better the preservation of brightness of the image.

RESULTS AND DISCUSSION

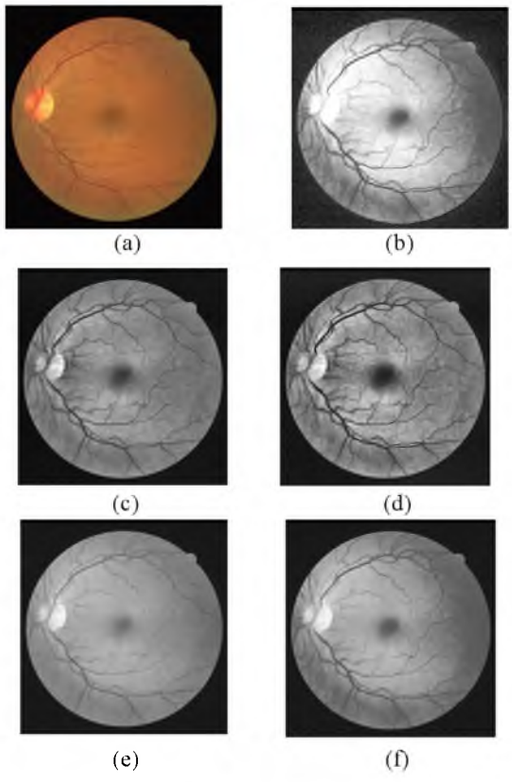

FIGURE 3. Fundus images of (a) Original image, and its respective enhanced image using (b) HE method, (c) AHE method, (d) CLAHE method, (e) BBCCE method and (f) DSI-BBCCE method.

TABLE 1. Mean and standard deviation of (PSNR) of different contrast enhancement (CE) methods consisting of HE, AHE, CLAHE, BBCCE and DSI-BBCCE on a total of 40 fundus images

CE methods	PSNR		
	Mean PSNR ± Std. Dev.	95% confidence interval for Mean	
		Lower Bound	Upper Bound
HE	13.40±1.84	12.81	13.99
AHE	23.36±1.23	22.97	23.76
CLAHE	19.54±1.12	19.18	19.90
BBCCE	19.27±1.42	18.81	19.73
DSI-BBCCE	20.08±0.94	19.78	20.38

TABLE 2. Mean and standard deviation of (AMBE) of different contrast enhancement methods consisting of HE, AHE, CLAHE, BBCCE and DSI-BBCCE on a total of 40 fundus images

CE methods	AMBE		
	Mean AMBE ± Std. Dev.	95% confidence interval for Mean	
		Lower Bound	Upper Bound
HE	43.92±13.27	39.67	48.17
AHE	9.95±4.59	8.48	11.42
CLAHE	14.66±7.02	12.41	16.90
BBCCE	25.65±3.67	24.47	26.82
DSI-BBCCE	20.15±1.89	19.54	20.75

TABLE 3. Mean and standard deviation of (SSIM) of different contrast enhancement methods consisting of HE, AHE, CLAHE, BBCCE and DSI-BBCCE on a total of 40 fundus images

CE methods	SSIM		
	Mean SSIM ± Std. Dev.	95% confidence interval for Mean	
		Lower Bound	Upper Bound
HE	0.4885±0.0681	0.4667	0.5103
AHE	0.7239±0.0105	0.7205	0.7273
CLAHE	0.5210±0.0160	0.5159	0.5261
BBCCE	0.8096±0.0185	0.8037	0.8155
DSI-BBCCE	0.8096±0.0185	0.8037	0.8155

TABLE 4. Mean and standard deviation of (SMO) of different contrast enhancement methods consisting of HE, AHE, CLAHE, BBCCE and DSI-BBCCE on a total of 40 fundus images

CE methods	SMO		
	Mean SMO ± Std. Dev.	95% confidence interval for Mean	
		Lower Bound	Upper Bound
HE	108.96±11.39	105.32	112.61
AHE	7.78±0.207	7.72	7.85
CLAHE	22.51±1.16	22.14	22.89
BBCCE	2.19±0.44	2.04	2.33
DSI-BBCCE	3.2±1.10	2.91	3.61

TABLE 5. Mean and standard deviation of (LMO) of different contrast enhancement methods consisting of HE, AHE, CLAHE, BBCCE and DSI-BBCCE on a total of 40 fundus images

CE methods	LMO		
	Mean LMO ± Std. Dev.	95% confidence interval for Mean	
		Lower Bound	Upper Bound
HE	1834.15±242.05	1756.74	1911.56
AHE	153.37±29.78	143.85	162.90
CLAHE	405.81±62.56	385.80	425.82
BBCCE	115.87±22.19	108.78	122.97
DSI-BBCCE	200.90±44.19	186.76	215.03

TABLE 6. One-way ANOVA computation by using different CE methods in PSNR, AMBE, SSIM, SMO and LMO

	Sum of squares	df	Mean square	F	P (Sig.)
PSNR					
Between groups	2073.847	4	518.462	283.377	< 0.001*
Within Groups	356.769	195	1.830		
Total	**2430.616**	**199**			
AMBE					
Between groups	27708.870	4	6927.217	131.240	<0.001*
Within Groups	10292.674	195	52.783		
Total	**38001.544**	**199**			
SSIM					
Between groups	3.881	4	0.970	850.951	< 0.001*
Within Groups	0.222	195	0.001		
Total	**4.103**	**199**			
SMO					
Between groups	330700.831	4	82675.208	3114.247	< 0.001*
Within Groups	5176.745	195	26.547		
Total	**335877.576**	199			
LMO					
Between groups	85486807.318	4	21371701.829	1623.091	< 0.001*
Within Groups	2567620.681	195	13167.286		
Total	**88054427.998**	**199**			

*Significant P value (P < 0.05)

TABLE 7. Overview of the mean and standard deviation of different CE methods

CE Methods	Mean ± Std. Dev.				
	PSNR	AMBE	SSIM	SMO	LMO
HE	13.40±1.84	43.92±13.27	0.4885±0.0681	108.96±11.39	1834.15±242.05
AHE	**23.36±1.23**	**9.95±4.59**	0.7239±0.0105	7.78±0.207	153.37±29.78
CLAHE	19.54±1.12	14.66±7.02	0.5210±0.0160	22.51±1.16	405.81±62.56
BBCCE	19.27±1.42	25.65±3.67	**0.8096±0.0185**	**2.19±0.44**	**115.87±22.19**
DSI-BBCCE	20.08±0.94	20.15±1.89	**0.8096±0.0185**	3.2±1.10	200.90±44.19

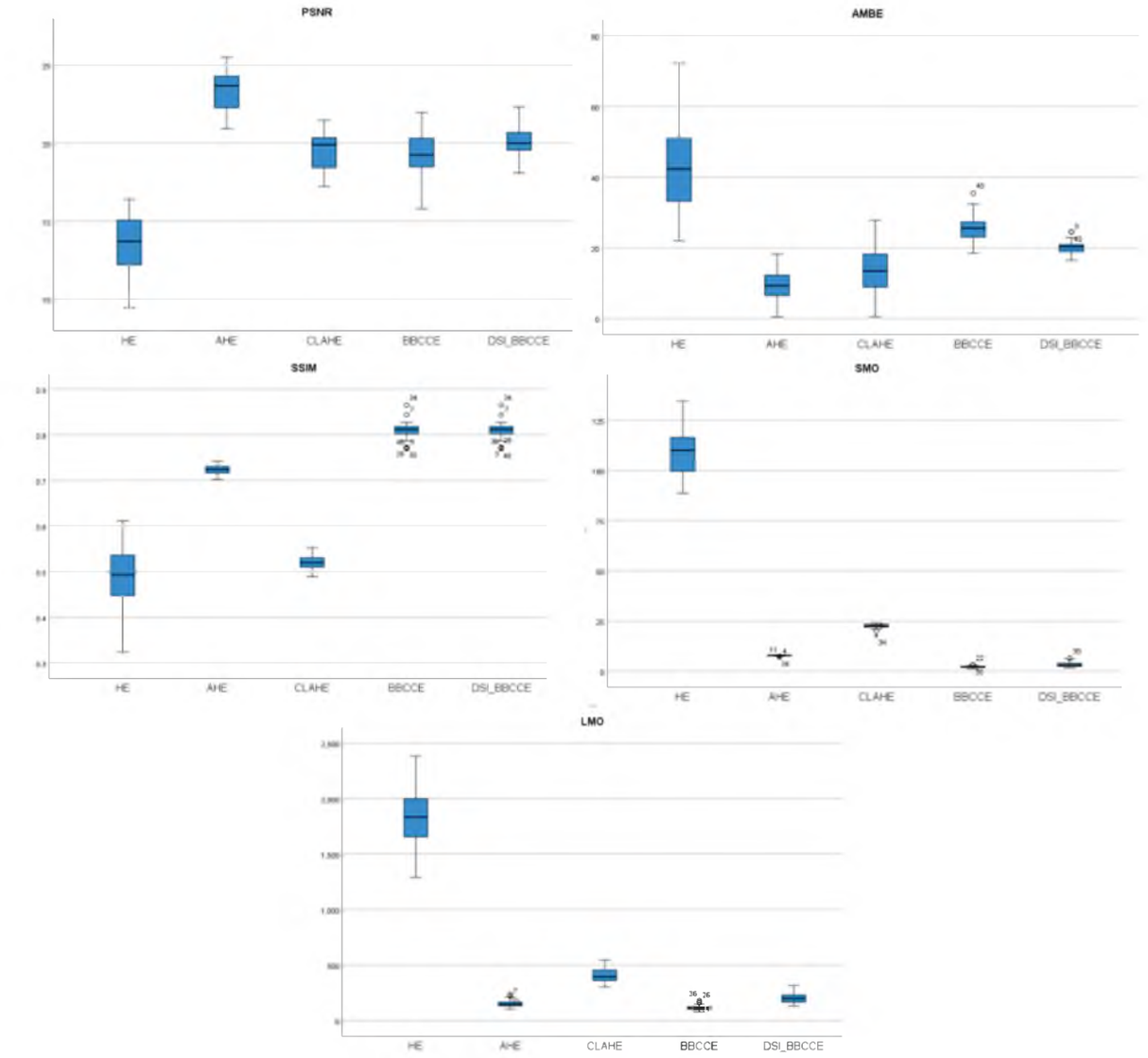

FIGURE 4. Boxplots of PSNR, AMBE, SSIM, SMO and LMO obtained from different contrast enhancement techniques using HE, AHE, CLAHE, BBCCE and DSI-BBCCE

TABLE 8. Multiple comparison of different CE methods using Fisher's Least Significant Difference (LSD) for PSNR

(I) Method	(J) Method	Mean difference ($I-J$)	Std. Error	P value (Sig.)	95% Confidence Interval	
					Lower bound	Upper bound
HE	AHE	-9.96*	0.3024552	0.001	-10.56	-9.37
	CLAHE	-6.14*	0.3024552	0.001	-6.74	-5.54
	BBCCE	-5.87*	0.3024552	0.001	-6.47	-5.27
	DSI-BBCCE	-6.68*	0.3024552	0.001	-7.28	-6.08
AHE	HE	9.96*	0.3024552	0.001	9.37	10.56
	CLAHE	3.83*	0.3024552	0.001	3.23	4.42
	BBCCE	4.09*	0.3024552	0.001	3.50	4.69
	DSI-BBCCE	3.28*	0.3024552	0.001	2.69	3.88
CLAHE	HE	6.14*	0.3024552	0.001	5.54	6.74
	AHE	-3.83*	0.3024552	0.001	-4.42	-3.23
	BBCCE	**0.27**	0.3024552	0.374	-0.33	0.87
	DSI-BBCCE	-0.54	0.3024552	0.075	-1.14	0.06
BBCCE	HE	5.87*	0.3024552	0.001	5.27	6.47
	AHE	-4.09*	0.3024552	0.001	-4.69	-3.50
	CLAHE	-0.27	0.3024552	0.374	-0.87	0.33
	DSI-BBCCE	-0.81*	0.3024552	0.008	-1.41	-0.21
DSI-BBCCE	HE	6.68*	0.3024552	0.001	6.08	7.28
	AHE	-3.28*	0.3024552	0.001	-3.88	-2.69
	CLAHE	**0.54**	0.3024552	0.075	-0.06	1.14
	BBCCE	0.81*	0.3024552	0.008	0.21	1.41

*. The mean difference is significant at the 0.05 level

TABLE 9. Multiple comparison of different CE methods using Fisher's Least Significant Difference (LSD) for AMBE

(I) Method	(J) Method	Mean difference ($I-J$)	Std. Error	P value (Sig.)	95% Confidence Interval	
					Lower bound	Upper bound
HE	AHE	33.97*	1.6245453	<0.001	30.77	37.18
	CLAHE	29.27*	1.6245453	<0.001	26.06	32.47
	BBCCE	18.27*	1.6245453	<0.001	15.07	21.48
	DSI-BBCCE	23.78*	1.6245453	<0.001	20.57	26.98
AHE	HE	-33.97*	1.6245453	<0.001	-37.18	-30.77
	CLAHE	-4.71*	1.6245453	0.004	-7.91	-1.50
	BBCCE	-15.70*	1.6245453	<0.001	-18.90	-12.49
	DSI-BBCCE	-10.20*	1.6245453	<0.001	-13.40	-6.99
CLAHE	HE	-29.27*	1.6245453	<0.001	-32.47	-26.06
	AHE	4.71*	1.6245453	0.004	1.50	7.91
	BBCCE	-10.99*	1.6245453	<0.001	-14.19	-7.79
	DSI-BBCCE	-5.49*	1.6245453	<0.001	-8.69	-2.29
BBCCE	HE	-18.27*	1.6245453	<0.001	-21.48	-15.07
	AHE	15.70*	1.6245453	<0.001	12.49	18.90
	CLAHE	10.99*	1.6245453	<0.001	7.79	14.19
	DSI-BBCCE	5.50*	1.6245453	<0.001	2.30	8.70
DSI-BBCCE	HE	-23.78*	1.6245453	<0.001	-26.98	-20.57
	AHE	10.20*	1.6245453	<0.001	6.99	13.40
	CLAHE	5.49*	1.6245453	<0.001	2.29	8.69
	BBCCE	-5.50*	1.6245453	<0.001	-8.70	-2.30

*. The mean difference is significant at the 0.05 level

TABLE 10. Multiple comparison of different CE methods using Fisher's Least Significant Difference (LSD) for SSIM

(I) Method	(J) Method	Mean difference ($I-J$)	Std. Error	P value (Sig.)	95% Confidence Interval	
					Lower bound	Upper bound
HE	AHE	-0.24*	0.0075502	<0.001	-0.25	-0.22
	CLAHE	-0.03*	0.0075502	<0.001	-0.05	-0.02
	BBCCE	-0.32*	0.0075502	<0.001	-0.33	-0.31
	DSI-BBCCE	-0.32*	0.0075502	<0.001	-0.33	-0.31
AHE	HE	0.24*	0.0075502	<0.001	0.22	0.25
	CLAHE	0.20*	0.0075502	<0.001	0.19	0.22
	BBCCE	-0.09*	0.0075502	<0.001	-0.10	-0.07
	DSI-BBCCE	-0.09*	0.0075502	<0.001	-0.10	-0.07
CLAHE	HE	0.03*	0.0075502	<0.001	0.01	0.04
	AHE	-0.20*	0.0075502	<0.001	-0.22	-0.19
	BBCCE	-0.29*	0.0075502	<0.001	-0.30	-0.27
	DSI-BBCCE	-0.29*	0.0075502	<0.001	-0.30	-0.27
BBCCE	HE	0.32*	0.0075502	<0.001	0.31	0.34
	AHE	0.09*	0.0075502	<0.001	0.07	0.10
	CLAHE	0.29*	0.0075502	<0.001	0.27	0.30
	DSI-BBCCE	**0.00**	0.0075502	1.000	-0.01	0.01
DSI-BBCCE	HE	0.32*	0.0075502	<0.001	0.31	0.34
	AHE	0.09*	0.0075502	<0.001	0.07	0.10
	CLAHE	0.29*	0.0075502	<0.001	0.27	0.30
	BBCCE	**0.00**	0.0075502	1.000	-0.01	0.015

*. The mean difference is significant at the 0.05 level

TABLE 11. Multiple comparison of different CE methods using Fisher's Least Significant Difference (LSD) for SMO

(I) Method	(J) Method	Mean difference ($I-J$)	Std. Error	P value (Sig.)	95% Confidence Interval	
					Lower bound	Upper bound
HE	AHE	101.18*	1.15212	<0.001	98.91	103.45
	CLAHE	86.45*	1.15212	<0.001	84.18	88.72
	BBCCE	106.77*	1.15212	<0.001	104.50	109.05
	DSI-BBCCE	105.70*	1.15212	<0.001	103.43	107.97
AHE	HE	-101.18*	1.15212	<0.001	-103.45	-98.91
	CLAHE	-14.73*	1.15212	<0.001	-17.00	-12.46
	BBCCE	5.60*	1.15212	<0.001	3.32	7.87
	DSI-BBCCE	4.52*	1.15212	<0.001	2.25	6.80
CLAHE	HE	-86.45*	1.15212	<0.001	-88.72	-84.18
	AHE	14.73*	1.15212	<0.001	12.46	17.00
	BBCCE	20.33*	1.15212	<0.001	18.05	22.60
	DSI-BBCCE	19.25*	1.15212	<0.001	16.98	21.53
BBCCE	HE	-106.77*	1.15212	<0.001	-109.05	-104.50
	AHE	-5.60*	1.15212	<0.001	-7.87	-3.32
	CLAHE	-20.33*	1.15212	<0.001	-22.60	-18.05
	DSI-BBCCE	**-1.07**	1.15212	0.353	-3.35	1.20
DSI-BBCCE	HE	-105.70*	1.15212	<0.001	-107.97	-103.43
	AHE	-4.52*	1.15212	<0.001	-6.80	-2.25
	CLAHE	-19.25*	1.15212	<0.001	-21.53	-16.98
	BBCCE	**1.07**	1.15212	0.353	-1.20	3.35

*. The mean difference is significant at the 0.05 level

TABLE 12. Multiple comparison of different CE methods using Fisher's Least Significant Difference (LSD) for LMO

(I) Method	(J) Method	Mean difference ($I-J$)	Std. Error	P value (Sig.)	95% Confidence Interval	
					Lower bound	Upper bound
HE	AHE	1680.78*	25.65861	<0.001	1630.18	1731.38
	CLAHE	1428.34*	25.65861	<0.001	1377.74	1478.95
	BBCCE	1718.28*	25.65861	<0.001	1667.68	1768.88
	DSI-BBCCE	1633.25*	25.65861	<0.001	1582.65	1683.86
AHE	HE	-1680.78*	25.65861	<0.001	-1731.38	-1630.18
	CLAHE	-252.44*	25.65861	<0.001	-303.04	-201.84
	BBCCE	**37.50**	25.65861	0.145	-13.10	88.10
	DSI-BBCCE	**-47.53**	25.65861	0.065	-98.13	3.08
CLAHE	HE	-1428.34*	25.65861	<0.001	-1478.95	-1377.74
	AHE	252.44*	25.65861	<0.001	201.84	303.04
	BBCCE	289.94*	25.65861	<0.001	239.33	340.54
	DSI-BBCCE	204.91*	25.65861	<0.001	154.31	255.52
BBCCE	HE	-1718.28*	25.65861	<0.001	-1768.88	-1667.68
	AHE	**-37.50**	25.65861	0.145	-88.10	13.10
	CLAHE	-289.94*	25.65861	<0.001	-340.54	-239.33
	DSI-BBCCE	-85.03*	25.65861	0.001	-135.63	-34.42
DSI-BBCCE	HE	-1633.25*	25.65861	<0.001	-1683.86	-1582.65
	AHE	**47.53**	25.65861	0.065	-3.08	98.13
	CLAHE	-204.91*	25.65861	<0.001	-255.52	-154.31
	BBCCE	85.03*	25.65861	0.001	34.42	135.63

*. The mean difference is significant at the 0.05 level

TABLE 13. Categorization of different CE methods into homogenous subset using the Duncan test for PSNR

Method	N	Subset for alpha = 0.05			
		1	2	3	4
HE	40	13.41			
BBCCE	40		19.28		
CLAHE	40		19.54	19.54	
DSI-BBCCE	40			20.09	
AHE	40				23.37
Sig.		1.00	0.374	0.07	1.00

Means for groups in homogenous subsets are displayed.
Harmonic Mean Sample Size = 40.00

TABLE 14. Categorization of different CE methods into homogenous subset using the Duncan test for AMBE

Method	N	Subset for alpha = 0.05				
		1	2	3	4	5
AHE	40	9.95				
CLAHE	40	153.37	14.66			
DSI-BBCCE	40			20.15		
BBCCE	40				25.65	
HE	40					43.93
Sig.		1.00	1.00	1.00	1.00	1.00

Means for groups in homogenous subsets are displayed.
Harmonic Mean Sample Size = 40.00

TABLE 15. Categorization of different CE methods into homogenous subset using the Duncan test for SSIM

Method	N	Subset for alpha = 0.05			
		1	2	3	4
HE	40	0.49			
CLAHE	40		0.52		
AHE	40			0.72	
BBCCE	40				0.81
DSI-BBCCE	40				0.81
Sig.		1.00	1.00	1.00	1.00

Means for groups in homogenous subsets are displayed.
Harmonic Mean Sample Size = 40.00

TABLE 16. Categorization of different CE methods into homogenous subset using the Duncan test for SMO

Method	N	Subset for alpha = 0.05			
		1	2	3	4
BBCCE	40	2.19			
DSI-BBCCE	40	3.27			
AHE	40		7.79		
CLAHE	40			22.52	
HE	40				108.97
Sig.		0.35	1.00	1.00	1.00

Means for groups in homogenous subsets are displayed.
Harmonic Mean Sample Size = 40.00

TABLE 17. Categorization of different CE methods into homogenous subset using the Duncan test for LMO

Method	N	Subset for alpha = 0.05			
		1	2	3	4
BBCCE	40	115.87			
AHE	40	153.37	153.37		
DSI-BBCCE	40		200.90		
CLAHE	40			405.81	
HE	40				1834.15
Sig.		0.145	0.065	1.00	1.00

Means for groups in homogenous subsets are displayed.
Harmonic Mean Sample Size = 40.00

TABLE 18. Ranking of methods in terms of PSNR, AMBE, SSIM, SMO and LMO according to Fisher's Least Significance (LSD) and the Duncan test

Rank	PSNR	AMBE	SSIM	SMO	LMO
1	AHE	AHE	**DSI-BBCCE**	BBCCE	BBCCE
2	**DSI-BBCCE**	CLAHE	AHE	**DSI-BBCCE**	AHE
3	CLAHE	**DSI-BBCCE**	CLAHE	AHE	**DSI-BBCCE**
4	BBCCE	BBCCE	BBCCE	CLAHE	CLAHE
5	HE	HE	HE	HE	HE

QUALITATIVE RESULTS

There are several factors to take account while accessing DSI-BBCCE enhanced image which are veins and background contrast enhancement, presence of image artifacts, natural looking and brightness preservation. In Figure 3(b), serious noise amplifications that can be seen in HE and in the black area beyond the fundus image. There are mild artifacts in Figure 3(c) and 3(d) enhanced using AHE and CLAHE respectively. There are no artifacts in Figure 3(e) and (f) which are enhanced using BBCCE and DSI-BBCCE.

For the natural looking and brightness preservation, HE 's brightness of the background fundus image is high that the boundary between optical disc and background cannot be differentiated as shown in Figure 3(a). For AHE in Figure 3(c), some parts of the background are bright and some regions are dark. The same goes to CLAHE in Figure 3(d) as if the background of the fundus has almost the same brightness intensity as the optic disc, the brightness of the fundus image is considered excessive. For BBCCE in Figure 3(e), the mean brightness of the background is the same overall. DSI-BBCCE in Figure 3(f) has two distinct mean brightness if compared with BBCCE in Figure 3(e) due to the more intensity levels shaded along the right sides and below.

The contrast between the veins and the background is affected by the brightness of the mean of the fundus. Figure 3(b), (c) and (d) has darker veins if compared to Figure 3(e) and (f) which has lighter veins. Figure 3(f) has a higher contrast between vein and background than in Figure 3(e). Figure 4 shows the boxplots of PSNR, AMBE, SSIM, SMO and LMO obtained from different contrast enhancement techniques using HE, AHE, CLAHE, BBCCE and DSI-BBCCE. It gives a clearer picture of comparison of the performance in terms of data distribution.

Based on an assessment done by Prof Wan Hazabbah, an ophthalmologist in Hospital Universiti Sains Malaysia (HUSM), important features such as cup-to-disk ratio and artery-to-vein (A/V) ratio in the fundus images are easier to be measured using the proposed DSI-BBCCE technique due to the strong structural similarity between the original image and the enhanced image.

STATISTICAL ANALYSIS

All tests are performed using SPSS (version 28). Table 1 shows the mean and standard deviation of PSNR of different contrast enhancement methods (HE, AHE, CLAHE, BBCCE and DSI-BBCCE) using 40 fundus images. Table 2 shows the mean and standard deviation of AMBE of different contrast enhancement methods (HE, AHE, CLAHE, BBCCE and DSI-BBCCE) using 40 fundus images. Table 3 shows the mean and standard deviation of SSIM of different contrast enhancement methods (HE, AHE, CLAHE, BBCCE and DSI-BBCCE) using 40 fundus images. Table 4 shows the mean and standard deviation of SMO of different contrast enhancement methods (HE, AHE, CLAHE, BBCCE and DSI-BBCCE) using 40 fundus images. Table 5 shows the mean and standard deviation of LMO of different contrast enhancement methods (HE, AHE, CLAHE, BBCCE and DSI-BBCCE) using 40 fundus images. PSNR assessed the power signal to noise ratio of an image. It is deduced that AHE (23.36±1.23) has the highest PSNR and followed by DSI-BBCCE (20.08±0.94). The performance of contrast enhancement methods from intensity distortion perspective is assessed by AMBE. AHE (9.95±4.59) produced the lowest AMBE mean, followed by CLAHE (14.66±7.02). DSI-BBCCE (20.15±1.89) ranked third in AMBE assessment. SSIM measures the similarity degree between original image and enhancement image. The higher the SSIM, the more similarity between the images. DSI-BBCCE (0.8096±0.0185) and BBCCE (0.8096±0.0185) achieved the same highest SSIM. SMO computes the structural difference. The smaller the SMO, the better the preservation of the image. BBCCE (2.19±0.44) has the smallest SMO, followed by DSI-BBCCE (3.2±1.10). LMO assessed the brightness preservation of the image, the smaller the LMO, the better the preservation of brightness of the image. BBCCE (115.87±22.19) achieved the lowest LMO, followed by AHE (153.37±29.78). DSI-BBCCE (200.90±44.19) ranked third in LMO assessment. Further analysis is performed to test the hypothesis.

Table 6 shows that the contrast enhancement methods imposed significantly different impact on the fundus images in all cases which are PSNR, AMBE, SSIM, SMO and LMO ($P < 0.05$). Therefore, the data is further analyzed using post hoc tests (Fisher's Least Significant Difference and the

Duncan test) so that the performance of different contrast enhancement methods can be evaluated.

Table 7 shows overview of the mean and standard deviation of different CE methods.

Table 8 shows that Fisher's least significant difference test indicates the mean differences between CLAHE and BBCCE (0.27; -0.27) which is insignificant in PSNR. With that, the other contrast enhancement methods have shown significant mean difference which is confirmed by Duncan test (Table 13), categorising CLAHE and DSI-BBCCE into the same subset.

Fisher's Least Significant Difference for AMBE (Table 9) show significant mean difference for all contrast enhancement methods while for SSIM, the mean difference between BBCCE and DSI-BBCCE (0.00; 0.00) is insignificant. Other contrast enhancement methods show significant difference. This can be confirmed by the Duncan test (Table 15) showing BBCCE and DSI-BBCCE in the same subset.

SMO's Fisher's Least Significant Difference (Table 11) shows that DSI-BBCCE and BBCCE has insignificant mean difference which can be confirmed by Duncan's test (Table 16) that shows they are in the same subset.

For Fisher's Least Significant Difference for LMO (Table 12), there are two insignificant mean difference which are (BBCCE and AHE) (37.50 and -37.50) and (DSI-BBCCE and AHE) (-47.53 and 47.53). The other contrast enhancement methods show significant mean difference.

The performance of contrast enhancement methods (HE, AHE, CLAHE, BBCCE and DSI-BBCCE) is ranked according to the results computed from PSNR, AMBE, SSIM, SMO and LMO in Table 18. From Table 18, it is found that DSI-BBCCE is ranked first in SSIM, ranked second in PSNR and SMO and ranked third in AMBE and LMO. Besides that, HE is the last for all experiments due to severe drawbacks from conventional histogram equalization to improve the contrast of fundus image.

Fundus images are prone to lose their image quality when they undergo enhancement such as structure preservation. The proposed technique, DSI-BBCCE is able to achieve the highest SSIM among all other techniques such as HE, AHE, CLAHE and BBCCE. Structure preservation of the features which are commonly assessed by clinician such as cup-to-disk ratio and artery-to-vein ratio can be better measured using the proposed technique.

CONCLUSION

In this paper, dualistic sub-image bi-histogram Bezier curve (DSI-BBCCE) is proposed to overcome the sudden increase in the cumulative density function graph which results in the over-enhancement. The median threshold is chosen instead of the conventional mean in BBCCE so that the threshold is not affected by large values and small values that either drive the mean upward or downward. The application of Bezier curves in the bi-histograms smoothen the cumulative density function graph providing gradual contrast in the fundus image. This method is proposed to assist ophthalmologists to distinguish the veins from the background in the fundus image for diagnosis. Overall, the performance of DSI-BBCCE is excellent in structural similarity between the original image and enhanced image, good in terms of power signal to noise ratio and natural preservation structure and averagely in terms of brightness preservation (AMBE and LMO).

ACKNOWLEDGEMENT

The authors are grateful to Universiti Teknologi Malaysia and Research Management Centre (RMC) for providing support under the Research University Grant (RUG), number R.J130000.7851.5F282.

DECLARATION OF COMPETING INTEREST

None

REFERENCES

Bowling, B. 2015. *Kanski's Clinical Ophthalmology E-Book: A Systematic Approach*: Elsevier Health Sciences.

Chai, H. Y., Swee, T. T., Seng, G. H., & Wee, L. K. 2013. Multipurpose contrast enhancement on epiphyseal plates and ossification centers for bone age assessment. *BioMedical Engineering OnLine* 12(1): 27. doi:10.1186/1475-925x-12-27

Cheung, C. Y.-l., Lamoureux, E., Ikram, M. K., Sasongko, M. B., Ding, J., Zheng, Y., . . . Wong, T. Y. (2012). Retinal vascular geometry in Asian persons with diabetes and retinopathy. *Journal of Diabetes Science and Technology* 6(3): 595-605.

Cheung, N., Rogers, S., Couper, D. J., Klein, R., Sharrett, A. R., & Wong, T. Y. 2007. Is diabetic retinopathy an independent risk factor for ischemic stroke? *Stroke* 38(2): 398-401.

Gan, H.-S., Swee, T. T., Karim, A., Helmy, A., Sayuti, K. A., Kadir, A., . . . Chaudhary, K. T. 2014. Medical image visual appearance improvement using bihistogram bezier curve contrast enhancement: data from the osteoarthritis initiative. *The Scientific World Journal*.

Ismail, N. H. B., Chen, S.-D., Ng, L. S., & Ramli, A. 2016. An analysis of image quality assessment algorithm to detect the presence of unnatural contrast enhancement.

Khan, Z. A., Beghdadi, A., Cheikh, F. A., Kaaniche, M., & Qureshi, M. A. 2020. *A Multi-Criteria Contrast Enhancement Evaluation Measure using Wavelet Decomposition.* Paper presented at the 2020 IEEE 22nd International Workshop on Multimedia Signal Processing (MMSP).

Kim, Y.-T. 1997. Contrast enhancement using brightness preserving bi-histogram equalization. *IEEE Transactions on Consumer Electronics* 43(1): 1-8.

Knudtson, M. D., Lee, K. E., Hubbard, L. D., Wong, T. Y., Klein, R., & Klein, B. E. 2003. Revised formulas for summarizing retinal vessel diameters. *Current Eye Research* 27(3): 143-149.

Lai, J., Wong, V., & Liew, G. 2019. Diabetic retinopathy and stroke. In *Diabetic Retinopathy and Cardiovascular Disease* (Vol. 27, pp. 38-53): Karger Publishers.

Lovic, D., Piperidou, A., Zografou, I., Grassos, H., Pittaras, A., & Manolis, A. 2020. The growing epidemic of diabetes mellitus. *Current Vascular Pharmacology* 18(2): 104-109. doi:10.2174/1570161117666190405165911

Ogurtsova, K., da Rocha Fernandes, J., Huang, Y., Linnenkamp, U., Guariguata, L., Cho, N., . . . Makaroff, L. 2017. IDF diabetes atlas: Global estimates for the prevalence of diabetes for 2015 and 2040. *Diabetes Research and Clinical Practice* 128: 40-50.

Teh, Y. M., Lim, S. K., Jusoh, N., Osman, K., & Mualif, S. A. 2021. CD80 Insights as Therapeutic Target in the Current and Future Treatment Options of Frequent-Relapse Minimal Change Disease. *BioMed Research International, 2021*.

Teh, Y. M., Mualif, S. A., & Lim, S. K. 2021. A comprehensive insight into autophagy and its potential signaling pathways as a therapeutic target in podocyte injury. *The International Journal of Biochemistry & Cell Biology* 106153.

Tian-Swee, T., Ameen, N. E., Hitam, W. H. W., Hum, Y.-C., & Teoh, C.-K. 2017. Preprocessing digital retinal images for vessel segmentation. *Research Journal of Applied Sciences, Engineering and Technology* 14(1): 1-6.

Wang, Y., Chen, Q., & Zhang, B. 1999. Image enhancement based on equal area dualistic sub-image histogram equalization method. *IEEE Transactions on Consumer Electronics* 45(1): 68-75.

WHO. 2021. Diabetes Statistics in Malaysia. https://gaiahealth.com.my/blogs/news/diabetes-statistics-in-malaysia

Wykoff, C. C., Khurana, R. N., Nguyen, Q. D., Kelly, S. P., Lum, F., Hall, R., . . . To, T. M. 2021. Risk of blindness among patients with diabetes and newly diagnosed diabetic retinopathy. *Diabetes Care*.

Yin, J. S. S., Swee, T. T., Yahya, A. B., Thye, M. T. F., Hiik, K. L. C., Meng, L. K., . . . Sayuti, K. A. B. 2020. Prominent region of interest contrast enhancement for knee MR Images: Data from the OAI. *Jurnal Kejuruteraan* 32(3): 145-155.